

Structure of the Bateman2 Domain of Yeast Snf4: Dimeric Association and Relevance for AMP Binding

Michael J. Rudolph,¹ Gabriele A. Amodeo,¹ Surtaj H. Iram,² Seung-Pyo Hong,² Giorgia Pirino,² Marian Carlson,² and Liang Tong^{1,*}

¹Department of Biological Sciences, Columbia University, New York, NY 10027, USA

²Department of Genetics and Development and Department of Microbiology, Columbia University, New York, NY 10032, USA

*Correspondence: ltong@columbia.edu

DOI 10.1016/j.str.2006.11.014

SUMMARY

AMP-activated protein kinase (AMPK) is a central regulator of energy homeostasis in mammals. AMP is believed to control the activity of AMPK by binding to the γ subunit of this heterotrimeric enzyme. This subunit contains two Bateman domains, each of which is composed of a tandem pair of cystathionine β -synthase (CBS) motifs. No structural information is currently available on this subunit, and the molecular basis for its interactions with AMP is not well understood. We report here the crystal structure at 1.9 Å resolution of the Bateman2 domain of Snf4, the γ subunit of the yeast ortholog of AMPK. The structure revealed a dimer of the Bateman2 domain, and this dimerization is supported by our light-scattering, mutagenesis, and biochemical studies. There is a prominent pocket at the center of this dimer, and most of the disease-causing mutations are located in or near this pocket.

INTRODUCTION

AMP-activated protein kinase (AMPK) is a central regulator of energy homeostasis in mammals (Carling, 2005; Hardie et al., 1998; Hardie and Sakamoto, 2006; Kahn et al., 2005; Kemp et al., 2003; Viollet et al., 2003). An elevated AMP:ATP concentration ratio (signifying energy depletion) leads to the activation of AMPK, which in turn shuts off energy-demanding, anabolic processes and stimulates energy-producing, catabolic processes. On the other hand, ATP is an inhibitor of AMPK activity. The therapeutic effects of metformin and rosiglitazone, two commonly used drugs against type 2 diabetes, are likely derived from their (indirect) activation of AMPK, making AMPK an important target for drug development against diabetes, obesity, and other diseases (Hardie and Sakamoto, 2006; Kahn et al., 2005).

AMPK is a heterotrimeric enzyme, consisting of one catalytic (α) and two regulatory (β and γ) subunits (Hardie

et al., 1998; Hardie and Sakamoto, 2006; Kahn et al., 2005). Different isoforms of these subunits exist in mammals ($\alpha 1$, $\alpha 2$, $\beta 1$, $\beta 2$, $\gamma 1$, $\gamma 2$, and $\gamma 3$), giving rise to the potential for many distinct AMPK complexes. The α subunit contains the Ser/Thr protein kinase domain (Hardie et al., 1998; Hardie and Sakamoto, 2006; Kahn et al., 2005), the crystal structure of which has recently been reported (Nayak et al., 2006; Rudolph et al., 2005), an autoinhibitory domain (Crute et al., 1998), and regions that are important for interacting with the regulatory subunits. The β subunit contains a glycogen-binding domain (Polekhina et al., 2005) and regions that are important for the formation of the trimeric complex.

The γ subunit contains four repeats of the cystathionine β -synthase (CBS) motif (Figure 1). CBS motifs contain about 60 amino acid residues and have been found in a variety of proteins from bacteria, archaea, and eukaryotes (Bateman, 1997). The motifs generally occur as tandem pairs, and each pair of CBS motifs is also known as a Bateman domain (Kemp, 2004). The γ subunit of mammalian AMPK therefore contains two Bateman domains (Bateman1 and Bateman2). It is currently believed that AMP regulates the activity of AMPK by binding to the γ subunit. AMP binding also promotes the phosphorylation of Thr172 in the activation loop of the kinase domain of the α subunit, and inhibits the dephosphorylation of this residue by phosphatases. Binding assays suggest that each Bateman domain can bind one AMP or ATP molecule, and the full-length γ subunit can bind two AMP molecules (Hardie and Sakamoto, 2006; Scott et al., 2004).

The functional importance of the CBS motifs is underscored by the observation that mutations in them have been linked to many human diseases (Hardie and Sakamoto, 2006; Kahn et al., 2005; Scott et al., 2004). For AMPK, mutations in the $\gamma 2$ subunit (R302Q, H383R, T400N, N488I, R531G, R531Q, and the insertion of a Leu after residue 350; Figure 1) are the cause of the Wolff-Parkinson-White (WPW) syndrome, which is characterized by arrhythmia, hypertrophy, and a glycogen storage disorder in the heart. In Hampshire pigs, an R200Q mutation in the $\gamma 3$ subunit, equivalent to the R302Q mutation in the $\gamma 2$ subunit (Figure 1), causes a glycogen storage disease in skeletal muscle (Milan et al., 2000). In comparison, the adjacent V199I polymorphism is associated with low

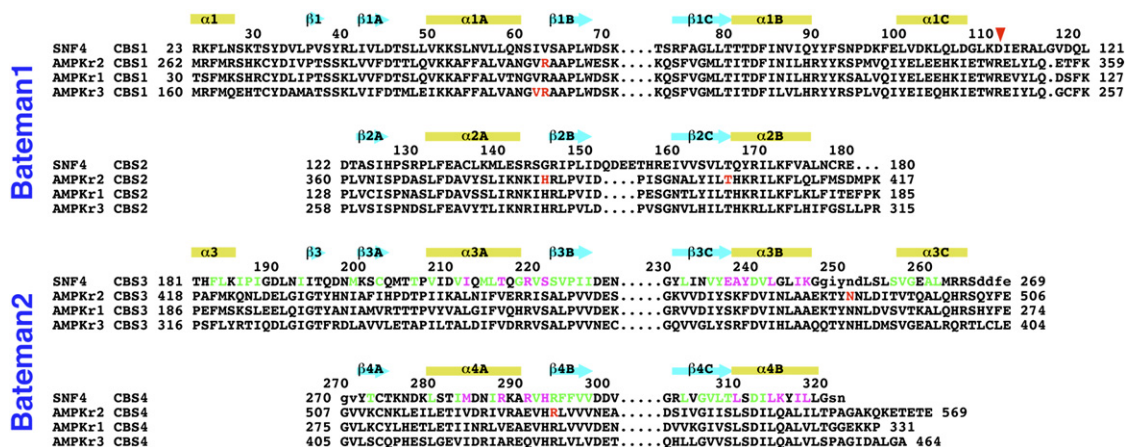


Figure 1. Sequence Alignment of Yeast Snf4 and Human AMPK γ 1, γ 2, and γ 3 Subunits

The secondary structure elements are labeled. Residues shown in green are in the hydrophobic core of the monomer, whereas those in magenta are in the dimer interface of the Bateman2 domain of Snf4. Residues shown in red are sites of disease-causing mutations, and the red arrowhead indicates the position of an insertion point. Equivalent residues in the four CBS motifs are aligned vertically.

glycogen level in skeletal muscle (Ciobanu et al., 2001). Mutations of CBS motifs in other proteins are linked to homocystinuria, retinitis pigmentosa, Bartter syndrome, and other diseases.

These mutations in the γ subunit may disrupt the activation of the kinase by AMP. Binding studies show that the mutations generally decrease the affinity between the γ subunit and AMP (Scott et al., 2004). Some of the mutations may also increase the basal activity of the kinase, which may explain the dominant, gain-of-function behavior of these mutations (Hamilton et al., 2001; Kahn et al., 2005).

In yeast, the ortholog of AMP-activated protein kinase, known as SNF1 (Hardie et al., 1998), has important roles in the transcription of genes repressed by glucose as well as in other biological processes. SNF1 also contains three subunits—the catalytic α subunit (Snf1) and the regulatory β (Sip1, Sip2, Gal83) and γ (Snf4) subunits. In contrast to mammalian AMPK, however, Snf4 does not appear to bind AMP (Hardie et al., 1998; Kahn et al., 2005), and how the SNF1 heterotrimer is activated remains unclear.

Crystal structures of several CBS motifs have been determined (Meyer and Dutzler, 2006; Miller et al., 2004; Zhang et al., 1999), but so far no structural information is available for the CBS motifs (Bateman domains) of AMPK. To provide a molecular basis for understanding the biochemical functions of the γ subunit, we have determined the crystal structure of the Bateman2 domain of Snf4 at 1.9 Å resolution. The structure revealed a dimeric association of the Bateman2 domain, and sequence analysis suggests that residues at the dimer interface are also conserved in the Bateman1 domain. The Bateman2 domain of yeast Snf4 shares 36% sequence identity with that of the mammalian γ 2 subunit, and our structure is therefore an excellent model for the mammalian Bateman domains. The structural information has implications for AMP binding by these domains.

RESULTS AND DISCUSSION

Overall Structure of the Bateman2 Domain of Snf4

The crystal structure of the Bateman2 domain (corresponding to the third and fourth CBS motifs) of yeast Snf4 has been determined at 1.9 Å resolution, based on a bacterial expression construct that contains residues 179–322 of the protein, Snf4(179–322). The refined structures have excellent agreement with the crystallographic data and the expected bond lengths, bond angles, and other geometric parameters (Table 1). The majority of the residues (92%) are in the most favored region of the Ramachandran plot, and none of the residues are in the disallowed region.

The current refined model in the native crystal contains residues 181–248, 253–265, and 272–320 of Snf4 (Figure 2A; see Figure S1 in the Supplemental Data available with this article online), while no electron density was observed for residues 249–252, 266–271, and those at the N and C termini of the recombinant protein (including the hexa-histidine tag at the C terminus). These residues are probably disordered in these crystals. The same segments of the protein are missing in the structure of the selenomethionyl protein. The monomers in these crystals have roughly the same conformation, with an rms distance of 0.5 Å for their equivalent C α atoms.

The structure shows that the CBS3 motif contains residues 198–269, while CBS4 contains 270–322 (Figure S1). Each motif contains a three-stranded antiparallel β sheet with helices on one side. The two CBS motifs have the same fold, with an rms distance of 0.7 Å for 47 pairs of C α atoms between them (Figure S1). They are related by a pseudo 2-fold axis (Figure S1), but the sequence identity among their structurally equivalent residues is 21%. The two motifs have strong interactions with each other, predominantly through the open face of their β sheets (Figure S1), as was observed originally in the structure of the

Table 1. Summary of Crystallographic Information

Protein	Native	Selenomethionyl
Space Group	<i>P</i> 3 ₂ 21	<i>F</i> 432
Maximum resolution (Å)	1.9	2.5
Number of observations	44,397	251,516
R _{merge} (%) ^a	6.1 (40.0)	9.8 (62.0)
I/σI	27.4 (3.5)	28.0 (5.9)
Resolution range used for refinement	55–1.9	50–2.5
Number of reflections ^b	11,241	19,087
Completeness (%)	100 (99)	99 (99)
R factor (%) ^c	20.4 (21.5)	23.9 (28.3)
Free R factor (%)	23.8 (27.7)	26.7 (33.6)
Rms deviation in bond lengths (Å)	0.015	0.010
Rms deviation in bond angles (°)	1.5	1.2
PDB accession code	2NYC	2NYE

^a $R_{\text{merge}} = \sum_h \sum_i |I_{hi} - \langle I_h \rangle| / \sum_h \sum_i I_{hi}$. The numbers in parentheses are for the highest resolution shell.

^b The number for the selenomethionyl protein includes both Friedel pairs.

^c $R = \sum_h |F_h^o - F_h^c| / \sum_h F_h^o$.

CBS motifs of inosine 5'-monophosphate dehydrogenase (IMPDH) (Zhang et al., 1999).

The structural similarity between CBS3 and CBS4 allowed us to produce an overall alignment of the four CBS motifs in the γ subunits of AMPK (Figure 1). We propose a systematic nomenclature for the secondary structure elements in these motifs, where for example the three β strands in CBS3 are named β 3A, β 3B, and β 3C and the three helices α 3A, α 3B, and α 3C (Figure 1).

Remarkably, residues 181–197, prior to CBS3 in the primary sequence, form a short helix (α 3) and a short β strand (β 3) in the structure and interact with residues in CBS4 (Figure 2A; Figure S1). The strand is hydrogen-bonded to β 4C in CBS4, extending that β sheet to four strands. It is likely that the conformations of these residues are maintained in the full-length Snf4 protein, as the Phe-Leu motif at the beginning of α 3 helps bury the hydrophobic core of CBS4 (Figure S1). Residues preceding CBS1 could also form a similar structure for the Bateman1 domain, as the Phe-Leu motif in the α 3 helix is also present in the segment preceding CBS1 (Figure 1). Therefore, the Bateman2 domain of Snf4 appears to cover residues 181–322, whereas the Bateman1 domain may contain residues 23–180 (Figure 1).

A Dimer of the Bateman2 Domain of Snf4

Our crystallographic analyses reveal a dimer of the Bateman2 domain of Snf4 (Figure 2A), and the same dimer is observed in both crystal forms of this protein. A total of 1400 Å² of the surface area of each monomer is buried at

the dimer interface, suggesting that the dimer should be stable. Light-scattering studies confirmed that the Bateman2 domain of Snf4 is dimeric in solution (Figure S2).

The dimer is formed by the head-to-tail arrangement of the two monomers, such that the CBS3 motif of one monomer is in contact with the CBS4 motif of the other monomer (Figure 2A). The overall shape of the dimer is similar to a disk, with a diameter of about 45 Å and a thickness of 25 Å (Figure 2B).

Most of the interactions at the dimer interface are mediated by the α A and α B helices in each CBS motif, and they form a four-helical bundle in the interface (Figure 2A). Each of these helices contains several exposed hydrophobic residues (Ile212 and Thr216 in α 3A; Tyr239, Leu242, and Ile245 in α 3B; Met284 in α 4A; and Leu310, Leu314, Ile317, and Leu318 in α 4B) (Figure 1), which become buried upon dimer formation (Figure 2C). In addition, the α A- β B loop in each CBS motif is positioned adjacent to the 2-fold axis of the dimer, and several functionally important residues (Ser221, His293, Arg294, and Thr309) are located in this region (Figure 2C, and see below). Residues in the dimer interface of the Bateman2 domain are also conserved in the Bateman1 domain (Figure 1).

Both head-to-head and head-to-tail dimeric associations of CBS tandem pairs have been observed for proteins from prokaryotic organisms, with unknown functions (Miller et al., 2004). These structures are exemplified by the Protein Data Bank entries 1PBJ and 1O50 (head-to-tail dimers; Figure 3A) and 1PVM and 1YAV (head-to-head dimers; Figure 3B). The structures of the head-to-tail dimers are remarkably similar to that of the Bateman2 domain of Snf4 (Figure S3). Moreover, all of these CBS tandem pairs contain an N-terminal extension, having a structure that is similar to that for residues 181–197 of Snf4 (Figure 2A; Figure S3).

A common feature of these dimeric CBS tandem pairs is the hydrophobic surface of the α A and α B helices, which mediates the self-association. In contrast, those CBS motifs that have a hydrophilic surface for these two helices, for example the CBS motifs of IMPDH (Zhang et al., 1999), are monomeric. An interesting example is observed in the structure of TM0892 from *Thermotoga maritima* (PDB entry 1VR9). The α A and α B helices in the second CBS motif have a hydrophobic surface and mediate its self-association in a tail-to-tail manner (Figure 3C). In contrast, the α A and α B helices in the first CBS motif have a hydrophilic surface, and they are splayed away from each other in the dimer (Figure 3C).

The CBS motifs of the CIC channel are also dimeric in solution (Meyer and Dutzler, 2006). A head-to-tail dimer similar to that observed for Snf4 here is proposed, although that CBS motif is monomeric in the crystal.

The Bateman Domains May Function as Dimers

To assess the stability of the observed dimer of the Snf4 Bateman2 domain, we mutated several residues in the dimer interface and expressed the L242E, R291A, H293E, R294Q, L314E single mutant proteins and the L242E/H293E, R291A/H293E, L242E/H293E/R291A double and

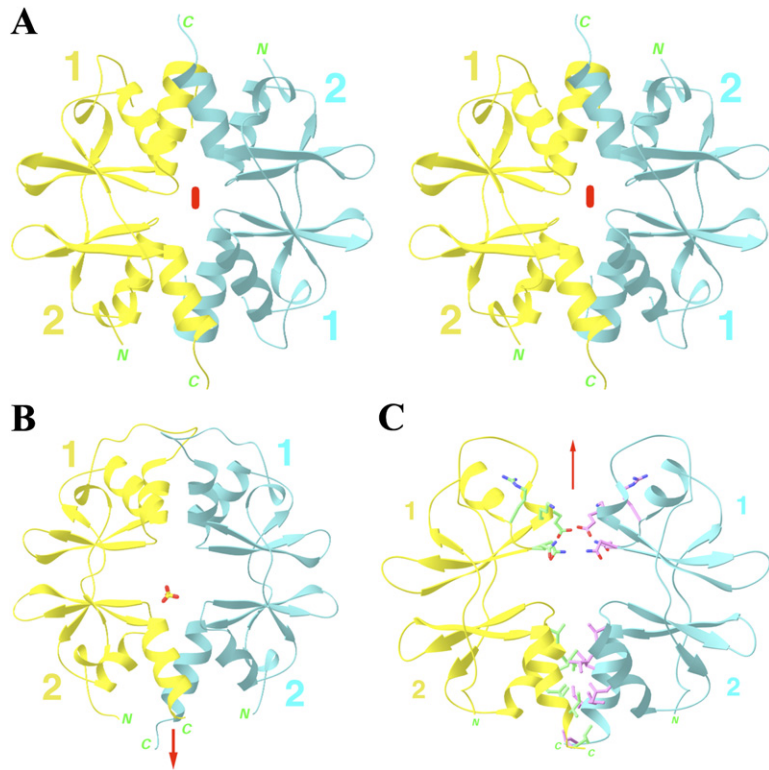


Figure 3. Structures of Representative Bateman Domain Dimers

(A) Structure of the head-to-tail dimer of TM0935 from *Thermotoga maritima* (PDB entry 1O50) (Miller et al., 2004).

(B) Structure of the head-to-head dimer of Ykul from *Bacillus subtilis* (PDB entry 1YAV).

(C) Structure of the tail-to-tail dimer of TM0892 from *Thermotoga maritima* (PDB entry 1VR9).

There are no interactions at the other half of the interface, as it is hydrophilic in nature. Produced with Ribbons (Carson, 1987).

with the stability of the dimer. Larger effects on the activity of SNF1 could be expected if the Bateman1 domain were mutated at the same time.

We also obtained experimental evidence for the self-association of full-length Snf4. HA- and LexA₈₇-tagged Snf4 were overexpressed from plasmids in *snf4Δ* mutant

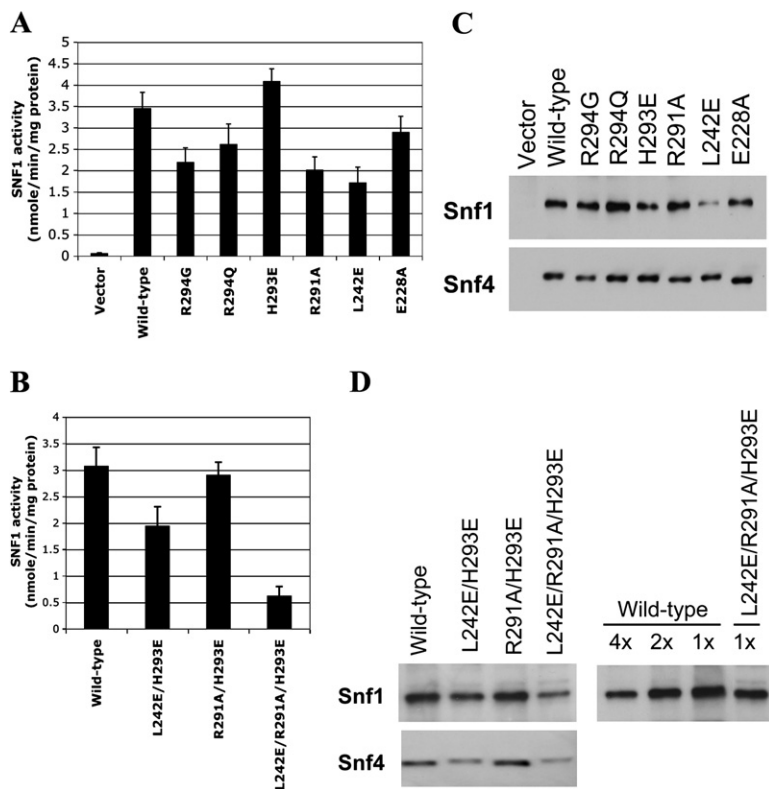


Figure 4. SNF1 Catalytic Activity Assay

(A) Wild-type and mutant Snf4 proteins, or no protein (vector pRS313), were expressed at native levels from plasmids in *snf4Δ* mutant yeast cells. Cells were grown in high glucose and collected by centrifugation, which activates SNF1 protein kinase. Three independent extracts were prepared, and SNF1 was assayed for phosphorylation of the SAMS peptide substrate.

(B) SNF1 activity assay, where the cells were collected by filtration, and resuspended in 0.05% glucose for 5 min to activate Snf1. Two independent extracts were assayed for SNF1 activity. Error bars are standard deviations for at least 6 assays.

(C) Fractions used in assays for (A) were analyzed by immunoblotting with anti-Snf1 and anti-Snf4.

(D) Fractions used in assays for (B) were analyzed by immunoblotting with anti-Snf1 and anti-Snf4. To compare levels of Snf1 protein in the wild-type and triple mutant extracts, 2-fold and 4-fold dilutions of the wild-type sample were loaded (right panel).

yeast cells lacking the native protein. HA-Snf4 was immunoprecipitated from cell lysates with anti-HA, and immunoblot analysis detected coprecipitation of a fraction of the LexA₈₇-Snf4 (Figure 5). In control experiments, no LexA₈₇-Snf4 was recovered from extracts containing HA alone. Similar results were obtained when cells were grown in abundant glucose or were subjected to glucose deprivation to activate SNF1 protein kinase. These findings are compatible with the model that Snf4 dimerizes in vivo. It remains possible that another protein (for example, Snf1 and/or one of the β subunits) mediated the association of the differently tagged proteins; however, Snf4 was overexpressed, whereas other proteins were present at endogenous levels. Overall, our structural and biochemical studies suggest that Snf4 and its Bateman domains may function as dimers.

A Model for the Bateman Domains of Mammalian AMPK

The Bateman2 domain of yeast Snf4 shares 36% sequence identity (52% similarity) with that of the γ 2 subunit of mammalian AMPK (Figure 1). Moreover, there are no gaps in this sequence alignment. Therefore, our structure of the Bateman2 domain of Snf4 is an excellent model for the mammalian Bateman2 domains. There are only a few noticeable differences between the mammalian and Snf4 Bateman2 domains in the dimer interface. For example, the Ala238 residue of Snf4 is replaced by a Lys or Arg in the mammalian γ subunits (Figure 1), which introduces an additional positive charge in this region (see below). These substitutions are unlikely to disrupt the dimer association.

The sequence homology between the Bateman2 and Bateman1 domains is much weaker (Figure 1), but they are expected to share significant structural similarity. Therefore, our structure of the Bateman2 domain of Snf4 should also be a good model for the Bateman1 domain of mammalian AMPK.

Implications for AMP Binding by the Bateman Domains

A model for the complex of AMP with the Bateman1 domain of the γ 1 subunit, based on the structure of IMPDH, was proposed earlier where the Bateman domain functions as a monomer (Adams et al., 2004). Our structural and biochemical studies suggest however that the γ subunit may be a dimer, with two disks for the two head-to-tail Bateman domain dimers, implying a $(\alpha\beta\gamma)_2$ stoichiometry for AMPK. While the native AMPK complex is believed to have the stoichiometry of $\alpha\beta\gamma$, a highly asymmetric shape was proposed to explain the observed MW of 230 kDa for this complex (Davies et al., 1994; Neumann et al., 2003), as the theoretical MW of this complex is only 130 kDa. It is possible that the observed MW actually corresponds to a dimer, $(\alpha\beta\gamma)_2$. Moreover, it has been suggested that the kinase domain of Snf1 also dimerizes (Nayak et al., 2006), although our data on this domain suggest this self association has low affinity (Rudolph et al., 2005).

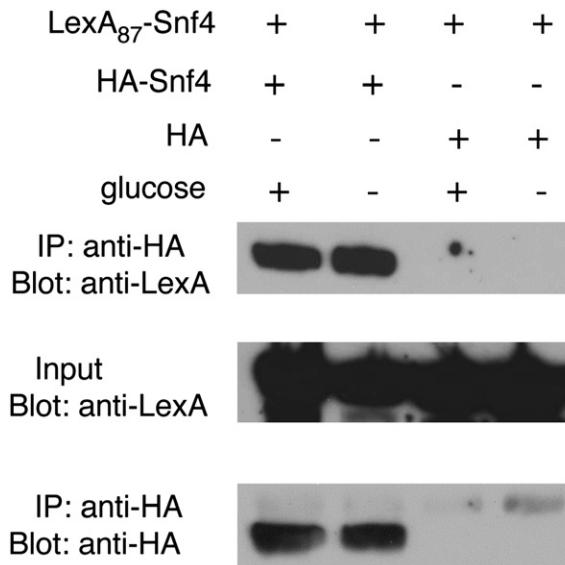


Figure 5. Coimmunoprecipitation Data Showing Self-Association of Snf4

Yeast cells (*snf4 Δ*) overexpressed LexA₈₇-Snf4 and HA-Snf4 or HA alone (vector). Cultures were grown in high glucose (+) or shifted for 5 min to glucose-limiting conditions (-), which activate Snf1 protein kinase. Cell lysates were prepared, and proteins were immunoprecipitated with anti-HA antibody. Immunoprecipitates (100 μ g) and input proteins (50 μ g) were subjected to immunoblot analysis with anti-HA and anti-LexA antibodies. The two upper panels are taken from the same exposure of the blot.

There is a prominent, electropositive pocket at the center of one face of the Bateman2 dimer disk (Figure 6A), while the other face is predominantly electronegative (Figure S4). This pocket could be the binding site for AMP or ATP (Figure 6B). This hypothesis is further supported by the fact that most of the disease-causing mutations are located in this pocket (Figure 6C). Binding studies show that these mutations generally reduce the affinity of the γ subunit for AMP (Scott et al., 2004). Therefore, this model would provide a molecular basis for the disease-causing effects of these mutations.

The possibility of a monomeric organization of the γ subunit, where the Bateman1 and Bateman2 domains directly contact each other and mimic a Bateman domain homodimer, cannot be excluded based on our data. The two domains are likely to be arranged in a head-to-head fashion in such a structure (Figure 6D), however, as the linker between them is not long enough to allow a head-to-tail dimer (Figure 6B). Such head-to-head dimers have been observed for bacterial CBS tandem pairs (Figure 3B), and can be formed by flipping one of the Bateman domains around its pseudo 2-fold axis (Figure 6D). This will split in half the pocket in the center of the head-to-tail dimer (Figure 6A), and there would instead be two smaller pockets, one on each face of the disk (Figure 6E).

Recent data suggest each γ subunit can bind two AMP or ATP molecules (Scott et al., 2004). The head-to-head

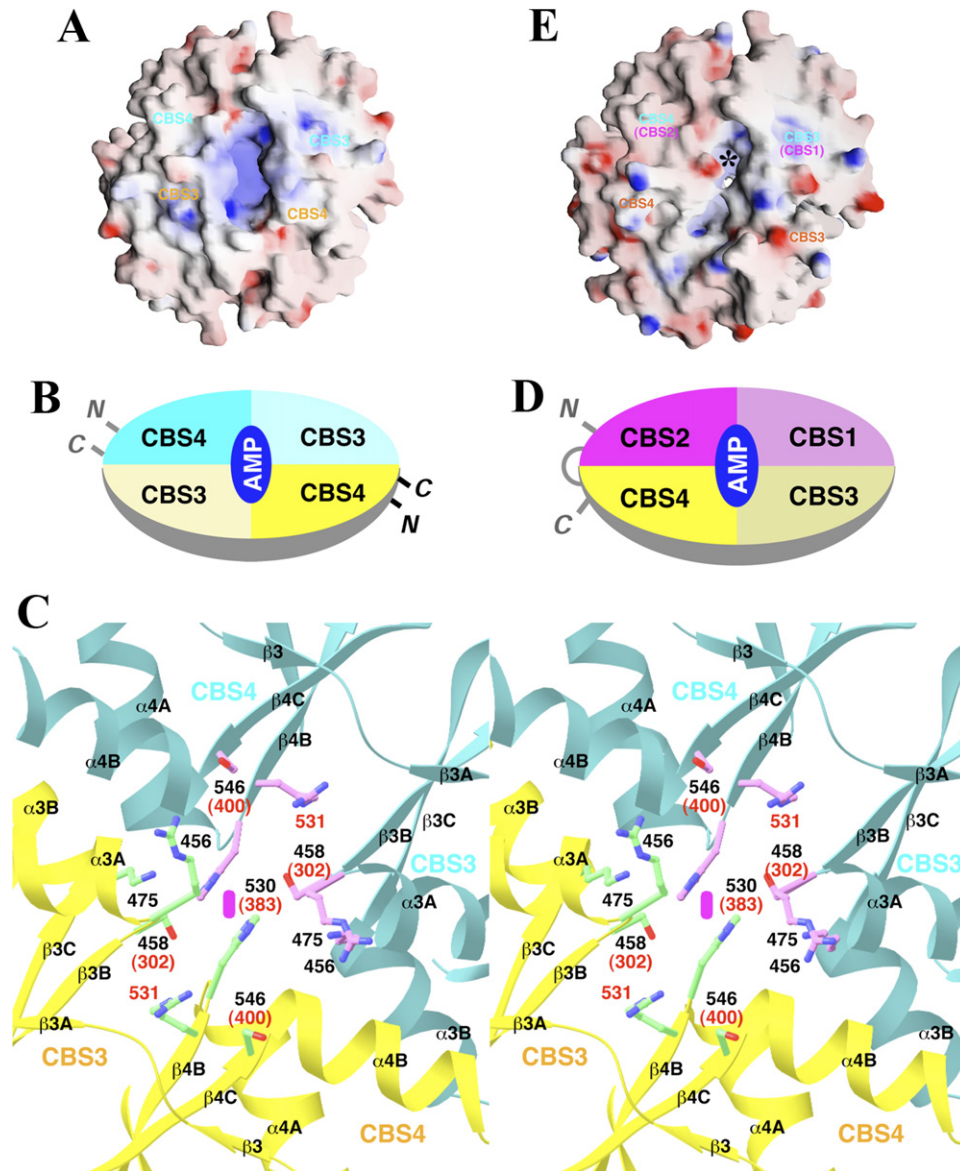


Figure 6. A Possible AMP Binding Pocket in the Center of the Bateman Domain Dimer

(A) Molecular surface of one face of the Bateman2 domain dimer of mammalian $\gamma 2$ subunit model.

(B) A cartoon of the head-to-tail Bateman domain dimer, and the proposed AMP-binding site in the center.

(C) Schematic drawing of the pocket in the center of the Bateman2 domain dimer of the $\gamma 2$ subunit. Residue numbers are for the Bateman2 domain, and those in parentheses are their equivalents in the Bateman1 domain. Residues that are sites of disease-causing mutations are labeled in red.

(D) A cartoon of the γ subunit monomer, with the two Bateman domains arranged in a head-to-head fashion. There is another binding site on the other face of the disk.

(E) Molecular surface of one face of the head-to-head dimer of the Bateman2 domain, representing the head-to-head organization of the γ subunit monomer. The star indicates the half pocket that is shared with that in the head-to-tail dimer. (A) and (E) were produced with Grasp (Nicholls et al., 1991), and (C) was produced with Ribbons (Carson, 1987).

monomeric organization of the γ subunit (Figure 6D) would be consistent with this stoichiometry, while the head-to-tail dimeric organization (Figure 6B) would not. Both models, however, suggest that the Bateman domains alone are dimeric, while a monomeric form of the domain was assumed in analyzing the binding data (Scott et al., 2004). Moreover, the Bateman domains were expressed as GST fusion proteins for the binding assays (Scott et al., 2004),

which is expected to enhance their dimerization. Further experiments are needed to reconcile this difference in stoichiometry between our model and the binding data.

Our model also provides an explanation why yeast Snf4 does not bind AMP. Sequence comparisons show that a His residue at the beginning of $\beta 2B$ in mammalian Bateman1 domain is replaced by a Gly residue in Snf4 (Figure 1). Mutation of this His residue in the $\gamma 1$ subunit to Gly (H151G,

equivalent to His530 in Figure 6C) is sufficient to render the mammalian AMPK complex insensitive to AMP (Adams et al., 2004). Moreover, a mutation at the equivalent position in the γ 2 subunit, H383R, is linked to the WPW disease. These observations may explain why the Bateman1 domain of Snf4 cannot bind AMP. In the Bateman2 domain, the largest difference between Snf4 and the mammalian γ subunits in this pocket is possibly the substitution of a Lys/Arg residue in the γ subunits (Lys475 in γ 2) by Ala238 in Snf4 (Figure 1). This additional positive charge may be a determining factor in AMP binding by the mammalian proteins. The natural ligand that activates the SNF1 complex in yeast remains to be identified.

In summary, we have determined the high-resolution structure of the Bateman2 domain of yeast Snf4. A dimeric association of this domain was revealed by the structure, which we have confirmed by solution light-scattering and mutagenesis studies. The Bateman domains therefore appear to function as dimers. We have identified a prominent pocket in the center of the dimer, which may be the binding site for AMP or ATP. This hypothesis is supported by the fact that most of the disease-causing mutations, which are known to reduce the affinity of the Bateman domain for the nucleotide, are located in this pocket. Our structural and functional studies provide molecular insights into the regulation of AMPK by the adenine nucleotides.

EXPERIMENTAL PROCEDURES

Protein Expression and Purification

Residues 179–322 of yeast Snf4, Snf4(179–322), containing CBS3 and CBS4 motifs, were subcloned into the pET26b vector and overexpressed in *E. coli* at 20°C. The soluble protein was purified by nickel affinity and gel filtration chromatography. The protein was concentrated to 10 mg/ml in a solution containing 50 mM Tris (pH 8.5), 100 mM NaCl, 5 mM DTT, and stored at –80°C. The recombinant protein contains a C-terminal hexa-histidine tag, which was not removed for crystallization.

The selenomethionyl protein was produced in B834(DE3) cells (Novagen), grown in defined LeMaster media supplemented with selenomethionine (Hendrickson et al., 1990), and purified following the same protocol as that for the native protein.

Protein Crystallization

Trigonal and cubic crystal forms of Snf4(179–322) were obtained. The trigonal crystal form was obtained with the native protein at 21°C by the sitting-drop vapor diffusion method. The protein was at 10 mg/ml concentration. The reservoir solution contained 100 mM NaAcetate (pH 4.5), 30% (w/v) PEG4000 and 200 mM (NH₄)Acetate. The crystal belongs to space group *P*3₂21, with cell parameters of $a = b = 64.2$ Å and $c = 61.1$ Å. There is one Snf4(179–322) molecule in the asymmetric unit.

The cubic crystal form was obtained with the selenomethionyl protein at 21°C by the sitting-drop vapor diffusion method. The protein was at 10 mg/ml concentration. The reservoir solution contained 100 mM NaAcetate (pH 4.5), 30% (w/v) PEG4000, 200 mM (NH₄)Formate, and 3% Benzamidine. The crystal belongs to space group *F*432, with cell parameters of $a = b = c = 235.6$ Å. There are two Snf4(179–322) molecules in the asymmetric unit.

The crystals were cryo-protected by the introduction of 20% (v/v) glycerol and flash-frozen in liquid nitrogen for data collection at 100K.

Data Collection and Processing

X-ray diffraction data were collected at the X4A and X4C beamlines of the National Synchrotron Light Source (NSLS). The diffraction images were processed with the HKL package (Otwinowski and Minor, 1997). A selenomethionyl single-wavelength anomalous diffraction (SAD) data set to 2.5 Å resolution was collected for the cubic form at the X4C beamline (Hendrickson, 1991). For structure refinement, a diffraction data set to 1.9 Å resolution was collected for the trigonal crystal at the X4A beamline. The data processing statistics are summarized in Table 1.

Structure Determination and Refinement

The Se sites were located using the SAD data with the program SnB (Weeks and Miller, 1999). The reflection phases were determined with the program Solve/Resolve (Terwilliger, 2003), which also automatically located about 80% of the residues. The atomic model was built with the program O (Jones et al., 1991). The trigonal crystal form was solved by the molecular replacement method using a monomer in the cubic form as the search model, with the program Molrep (Vagin and Teplyaev, 2000). The structure refinement was carried out with the programs CNS (Brunger et al., 1998) and Refmac5 (Murshudov et al., 1997). The statistics on the structure refinement are summarized in Table 1.

Mutagenesis

Mutants of Snf4 were created with the QuikChange kit (Stratagene) and verified by sequencing. The mutant proteins were purified following the same protocol as the wild-type enzyme.

SNF1 Assays

Centromeric plasmid pOV75 expresses Snf4 from the native promoter; this plasmid contains a NotI site at the C terminus of the ORF and differs from pOV76 (Vincent et al., 2001) in lacking GFP sequence. Wild-type and mutant Snf4 proteins were expressed from pOV75 and its mutant derivatives in *Saccharomyces cerevisiae* strain MCY2634 (*snf4* Δ 2). Cultures were grown to mid-log phase in selective synthetic complete medium containing 2% glucose. Cells were collected by centrifugation, which activates Snf1 protein kinase, or were collected by filtration, shifted to 0.05% glucose for 5 min, and collected by filtration. Extracts were prepared from at least two independent cultures, and Snf1 was partially purified and assayed, at different protein concentrations, for phosphorylation of the SAMS peptide (Davies et al., 1989), as described (Hedbacker et al., 2004). Kinase activity is expressed as nanomoles of phosphate incorporated into the peptide per minute per milligram of protein. Assayed fractions were subjected to immunoblot analysis with anti-Snf1 (Celenza and Carlson, 1986) and anti-Snf4 (Estruch et al., 1992) antibodies.

Coimmunoprecipitation Studies

Proteins were expressed in *Saccharomyces cerevisiae* strain MCY5803 (*snf4* Δ ::*kanMX4*). Snf4, tagged at the N terminus with a triple HA epitope or the DNA binding domain of LexA (LexA₈₇), was expressed from the strong *ADH1* promoter from plasmid pGP2 (derivative of vector pWS93) or pRJ58 (Jiang and Carlson, 1996), respectively. Cultures were grown to mid-log phase in selective synthetic complete medium containing 2% glucose. Cells were collected by filtration and frozen at –80°C or shifted to 0.05% glucose for 5 min, collected, and frozen. Preparation of protein lysates and immunoprecipitation were as described (Treitel et al., 1998). Protein (200 μ g) was immunoprecipitated with anti-HA (12CA5) and collected with rProtein A immobilized on beads (RepliGen). Proteins were separated by electrophoresis in 12% SDS-polyacrylamide and subjected to immunoblot analysis with anti-HA and anti-LexA (Invitrogen). Antibody was detected with ECL Plus (Amersham).

Supplemental Data

Supplemental Data include four figures and are available at <http://www.structure.org/cgi/content/full/15/1/65/DC1/>.

ACKNOWLEDGMENTS

We thank Randy Abramowitz and John Schwanof for setting up the X4A and X4C beamlines at the NSLS. This research is supported in part by a grant from the NIH to L.T. and in part by NIH grant GM34095 to M.C. G.A.A. was supported by an NIH training program in molecular biophysics (GM08281).

Received: October 17, 2006

Revised: November 20, 2006

Accepted: November 20, 2006

Published: January 16, 2007

REFERENCES

- Adams, J., Chen, Z.-P., van Denderen, B.J.W., Morton, C.J., Parker, M.W., Witters, L.A., Stapleton, D., and Kemp, B.E. (2004). Intrasteric control of AMPK via the g1 subunit AMP allosteric regulatory site. *Protein Sci.* **13**, 155–165.
- Bateman, A. (1997). The structure of a domain common to archaeobacteria and the homocystinuria disease protein. *Trends Biochem. Sci.* **22**, 12–13.
- Brunger, A.T., Adams, P.D., Clore, G.M., DeLano, W.L., Gros, P., Grosse-Kunstleve, R.W., Jiang, J.-S., Kuszewski, J., Nilges, M., Pannu, N.S., et al. (1998). Crystallography & NMR system: a new software suite for macromolecular structure determination. *Acta Crystallogr. D Biol. Crystallogr.* **54**, 905–921.
- Carling, D. (2005). AMP-activated protein kinase: balancing the scales. *Biochimie* **87**, 87–91.
- Carson, M. (1987). Ribbon models of macromolecules. *J. Mol. Graph.* **5**, 103–106.
- Celenza, J.L., and Carlson, M. (1986). A yeast gene that is essential for release from glucose repression encodes a protein kinase. *Science* **233**, 1175–1180.
- Ciobanu, D., Bastiaansen, J., Malek, M., Helm, J., Woollard, J., Plastow, G., and Rothschild, M. (2001). Evidence for new alleles in the protein kinase adenosine monophosphate-activated g3-subunit gene associated with low glycogen content in pig skeletal muscle and improved meat quality. *Genetics* **159**, 1151–1162.
- Crute, B.E., Seefeld, K., Gamble, J., Kemp, B.E., and Witters, L.A. (1998). Functional domains of the a1 catalytic subunit of the AMP-activated protein kinase. *J. Biol. Chem.* **273**, 35347–35354.
- Davies, S.P., Carling, D., and Hardie, D.G. (1989). Tissue distribution of the AMP-activated protein kinase, and lack of activation by cyclic-AMP-dependent protein kinase, studied using a specific and sensitive assay. *Eur. J. Biochem.* **186**, 123–128.
- Davies, S.P., Hawley, S.A., Woods, A., Carling, D., Haystead, T.A.J., and Hardie, D.G. (1994). Purification of the AMP-activated protein kinase on ATP-g-sepharose and analysis of its subunit structure. *Eur. J. Biochem.* **223**, 351–357.
- Estruch, F., Treitel, M.A., Yang, X., and Carlson, M. (1992). N-terminal mutations modulate yeast SNF1 protein kinase function. *Genetics* **132**, 639–650.
- Hamilton, S.R., Stapleton, D., O'Donnell, J.B., Jr., Kung, J.T., Dalal, S.R., Kemp, B.E., and Witters, L.A. (2001). An activating mutation in the g1 subunit of the AMP-activated protein kinase. *FEBS Lett.* **500**, 163–168.
- Hardie, D.G., and Sakamoto, K. (2006). AMPK: a key sensor of fuel and energy status in skeletal muscle. *Physiology* **21**, 48–60.
- Hardie, D.G., Carling, D., and Carlson, M. (1998). The AMP-activated/SNF1 protein kinase subfamily: metabolic sensors of the eukaryotic cell? *Annu. Rev. Biochem.* **67**, 821–855.
- Hedbacker, K., Hong, S.-P., and Carlson, M. (2004). Pak1 protein kinase regulates activation and nuclear localization of Snf1-Gal83 protein kinase. *Mol. Cell. Biol.* **24**, 8255–8263.
- Hendrickson, W.A. (1991). Determination of macromolecular structures from anomalous diffraction of synchrotron radiation. *Science* **254**, 51–58.
- Hendrickson, W.A., Horton, J.R., and LeMaster, D.M. (1990). Selenomethionyl proteins produced for analysis by multiwavelength anomalous diffraction (MAD): a vehicle for direct determination of three-dimensional structure. *EMBO J.* **9**, 1665–1672.
- Jiang, R., and Carlson, M. (1996). Glucose regulates protein interactions within the yeast SNF1 protein kinase complex. *Genes Dev.* **10**, 3105–3115.
- Jones, T.A., Zou, J.Y., Cowan, S.W., and Kjeldgaard, M. (1991). Improved methods for building protein models in electron density maps and the location of errors in these models. *Acta Crystallogr. A* **47**, 110–119.
- Kahn, B.B., Alquier, T., Carling, D., and Hardie, D.G. (2005). AMP-activated protein kinase: ancient energy gauge provides clues to modern understanding of metabolism. *Cell Metab.* **1**, 15–25.
- Kemp, B.E. (2004). Bateman domains and adenosine derivatives form a binding contract. *J. Clin. Invest.* **113**, 182–184.
- Kemp, B.E., Stapleton, D., Campbell, D.J., Chen, Z.-P., Murthy, S., Walter, M., Gupta, A., Adams, J.J., Katsis, F., van Denderen, B., et al. (2003). AMP-activated protein kinase, super metabolic regulator. *Biochem. Soc. Trans.* **31**, 162–168.
- Meyer, S., and Dutzler, R. (2006). Crystal structure of the cytoplasmic domain of the chloride channel ClC-0. *Structure* **14**, 299–307.
- Milan, D., Jeon, J.-T., Looft, C., Amarger, V., Robic, A., Thelander, M., Rogel-Gaillard, C., Paul, S., Iannuccelli, N., Rask, L., et al. (2000). A mutation in PRKAG3 associated with excess glycogen content in pig skeletal muscle. *Science* **288**, 1248–1251.
- Miller, M.D., Schwarzenbacher, R., von Delft, F., Abdubek, P., Ambing, E., Biorac, T., Brinen, L.S., Canaves, J.M., Cambell, J., Chiu, H.-J., et al. (2004). Crystal structure of a tandem cystathionine- β -synthase (CBS) domain protein (TM0935) from *Thermotoga maritima* at 1.87 Å resolution. *Proteins* **57**, 213–217.
- Murshudov, G.N., Vagin, A.A., and Dodson, E.J. (1997). Refinement of macromolecular structures by the maximum-likelihood method. *Acta Crystallogr. D Biol. Crystallogr.* **53**, 240–255.
- Nayak, V., Zhao, K., Wyce, A., Schwartz, M.F., Lo, W.S., Berger, S.L., and Marmorstein, R. (2006). Structure and dimerization of the kinase domain from yeast Snf1, a member of the Snf1/AMPK protein family. *Structure* **14**, 477–485.
- Neumann, D., Woods, A., Carling, D., Wallimann, T., and Schlattner, U. (2003). Mammalian AMP-activated protein kinase: functional, heterotrimeric complexes by co-expression of subunits in *Escherichia coli*. *Protein Expr. Purif.* **30**, 230–237.
- Nicholls, A., Sharp, K.A., and Honig, B. (1991). Protein folding and association: insights from the interfacial and thermodynamic properties of hydrocarbons. *Proteins* **11**, 281–296.
- Otwinowski, Z., and Minor, W. (1997). Processing of X-ray diffraction data collected in oscillation mode. *Methods Enzymol.* **276**, 307–326.
- Polekhina, G., Gupta, A., van Denderen, B.J., Feil, S.C., Kemp, B.E., Stapleton, D., and Parker, M.W. (2005). Structural basis for glycogen recognition by AMP-activated protein kinase. *Structure* **13**, 1453–1462.
- Rudolph, M.J., Amodeo, G.A., Bai, Y., and Tong, L. (2005). Crystal structure of the protein kinase domain of yeast AMP-activated protein kinase Snf1. *Biochem. Biophys. Res. Commun.* **337**, 1224–1228.
- Scott, J.W., Hawley, S.A., Green, K.A., Anis, M., Stewart, G., Scullion, G.A., Norman, D.G., and Hardie, D.G. (2004). CBS domains form energy-sensing modules whose binding of adenosine ligands is disrupted by disease mutations. *J. Clin. Invest.* **113**, 274–284.

Crystal Structure of the Bateman2 Domain of Snf4

- Terwilliger, T.C. (2003). SOLVE and RESOLVE: automated structure solution and density modification. *Methods Enzymol* 374, 22–37.
- Treitel, M.A., Kuchin, S., and Carlson, M. (1998). Snf1 protein kinase regulates phosphorylation of the Mig1 repressor in *Saccharomyces cerevisiae*. *Mol. Cell. Biol.* 18, 6273–6280.
- Vagin, A.A., and Teplyakov, A. (2000). An approach to multi-copy search in molecular replacement. *Acta Crystallogr. D Biol. Crystallogr.* 56, 1622–1624.
- Vincent, O., Townley, R., Kuchin, S., and Carlson, M. (2001). Subcellular localization of the Snf1 kinase is regulated by specific beta subunits and a novel glucose signaling mechanism. *Genes Dev.* 15, 1104–1114.
- Viollet, B., Andreelli, F., Jorgensen, S.B., Perrin, C., Flamez, D., Mu, J., Wojtaszewski, J.F.P., Schuit, F.C., Birnbaum, M., Richter, E., et al. (2003). Physiological role of AMP-activated protein kinase (AMPK): insights from knockout mouse models. *Biochem. Soc. Trans.* 31, 216–219.
- Weeks, C.M., and Miller, R. (1999). The design and implementation of SnB v2.0. *J. Appl. Crystallogr.* 32, 120–124.
- Zhang, R.-G., Evans, G., Rotella, F.J., Westbrook, E.M., Beno, D., Huberman, E., Joachimiak, A., and Collart, F.R. (1999). Characteristics and crystal structure of bacterial inosine-5'-monophosphate dehydrogenase. *Biochemistry* 38, 4691–4700.